

# Accepted Manuscript

Title: Structural Analysis and Electrochemical Performance of  $\text{Li}_2\text{CoPO}_4\text{F}$  Cathode Materials

Author: Quang Duc Truong Murukanahally K. Devaraju  
Yoshiyuki Ganbe Takaaki Tomai Itaru Honma



PII: S0013-4686(14)00328-4

DOI: <http://dx.doi.org/doi:10.1016/j.electacta.2014.02.026>

Reference: EA 22187

To appear in: *Electrochimica Acta*

Received date: 22-11-2013

Revised date: 5-2-2014

Accepted date: 7-2-2014

Please cite this article as: Quang Duc Truong Murukanahally K. Devaraju Yoshiyuki Ganbe Takaaki Tomai Itaru Honma Structural Analysis and Electrochemical Performance of  $\text{Li}_2\text{CoPO}_4\text{F}$  Cathode Materials (2014), <http://dx.doi.org/10.1016/j.electacta.2014.02.026>

This is a PDF file of an unedited manuscript that has been accepted for publication. As a service to our customers we are providing this early version of the manuscript. The manuscript will undergo copyediting, typesetting, and review of the resulting proof before it is published in its final form. Please note that during the production process errors may be discovered which could affect the content, and all legal disclaimers that apply to the journal pertain.

# Structural Analysis and Electrochemical Performance of Li<sub>2</sub>CoPO<sub>4</sub>F Cathode Materials

Quang Duc Truong\*, Murukanahally K. Devaraju, Yoshiyuki Ganbe, Takaaki Tomai, Itaru Honma\*

Institute of Multidisciplinary Research for Advanced Materials, Tohoku University, Sendai 980-8577, Japan.

**Corresponding Author:** Tel./Fax: 81-22-217 5815.

\*Email address: (Q.D.T) tqduc@mail.tagen.tohoku.ac.jp; (I.H.) i.honma@tagen.tohoku.ac.jp

## ABSTRACT

Li<sub>2</sub>CoPO<sub>4</sub>F cathode materials have been synthesized by a two-step method combining a sol-gel route and solid state reaction. X-ray diffraction (XRD) analysis confirmed that the LiCoPO<sub>4</sub>F was well-crystallized in orthorhombic crystal structure with *Pnma* space group. From the high resolution transmission electron microscopy (HRTEM) image, the lattice fringes of {001} and {100} are well-resolved. HRTEM image and selected area electron diffraction (SAED) pattern reveal the highly crystalline nature of Li<sub>2</sub>CoPO<sub>4</sub>F having an ordered orthorhombic crystal structure. The Co atoms chains of Li<sub>2</sub>CoPO<sub>4</sub>F have been observed using high angle annular dark-field scanning transmission electron microscopy (HAADF-STEM). The Raman and FTIR spectra indicate the symmetry and stability of the Li<sub>2</sub>CoPO<sub>4</sub>F structure. The Li<sub>2</sub>CoPO<sub>4</sub>F cathode materials delivered an initial discharge capacity of 91 mAhg<sup>-1</sup> at C/10 rate with good

cyclic performance. The discharge profile of  $\text{LiCoPO}_4$  shows a plateau at 5.0 V, revealing its importance as high potential voltage cathode.

KEYWORDS: Lithium-ion batteries,  $\text{Li}_2\text{CoPO}_4\text{F}$ , structural analysis, electrochemistry.

## 1. Introduction

Rechargeable lithium-ion batteries are considered to be most promising storage system for novel energy storage systems and future application in hybrid electric vehicles (HEV) or electric vehicles (EV). To realize the application of lithium-ion batteries suitable for a large scale, cathode materials with high energy densities and high power densities, are desirable.<sup>1,2</sup> New research field has been directed to improve the energy densities and power densities of the high-voltage cathode materials. Recently, fluoro-oxyanions frameworks have been proposed as high-energy-density materials due to their high ionicity of M-F bond and resulting higher operating potential [3-5]. Furthermore, the potential extraction of two lithium ions can be realized which makes them to be promising high-capacity cathode materials for high-energy density batteries ( $290 \text{ mAhg}^{-1}$ ). To date, several fluorophosphates have been investigated as frameworks for reversible extraction/insertion of lithium ions [6-11]. Particularly, lithium fluorophosphates of formula  $\text{Li}_2\text{MPO}_4\text{F}$  (M = Fe, Mn, Co, Ni) are of importance [10-12], in which lithium cobalt fluorophosphates  $\text{Li}_2\text{CoPO}_4\text{F}$  has attracted attention since it offers very high redox potential at approximately 5.1 V versus  $\text{Li}/\text{Li}^+$  and high theoretical capacity ( $287 \text{ mAhg}^{-1}$ ) with possible extraction of two lithium ions per formula unit [13-20]. Recently, research has been focused on  $\text{Li}_2\text{CoPO}_4\text{F}$  in different aspects such as synthesis, electrochemical performance and crystal structure change

during the charge/discharge cycle. Understanding of crystal structures of cathode materials, especially multi-element compounds such as  $\text{Li}_2\text{CoPO}_4\text{F}$  is of particular importance to improve the electrochemical performance. This is due to the fact that the crystal structure, surface chemistry and chemical composition of the cathode materials are crucial factor affecting the insertion and extraction of Li ions from the frameworks.

In this paper, we report the synthesis, characterization and investigation on the  $\text{Li}_2\text{CoPO}_4\text{F}$  particles using the high-resolution transmission electron microscopy (HRTEM), selected area electron diffraction (SAED), energy dispersive X-ray spectrometry (EDS), and elemental compositional mapping using high-angle angular dark field scanning transmission electron microscopy (HAADF-STEM) and local structure and chemical bonding using Raman spectroscopy and Fourier transform infrared spectroscopy (FTIR). The  $\text{Li}_2\text{CoPO}_4\text{F}$  materials were also tested as cathode materials for lithium-ion batteries, and an initial discharge capacity of  $91 \text{ mAhg}^{-1}$  at C/10 rate was obtained with good cyclic performance.

## 2. Experimental

$\text{Li}_2\text{CoPO}_4\text{F}$  was synthesized by two-step process combining sol-gel method with solid-state route. Firstly,  $\text{LiCoPO}_4$  materials were directly synthesized by a facile sol-gel method with a simple treatment in air atmospheres according to our previous report [21]. Typically,  $\text{LiNO}_3$ ,  $\text{Co}(\text{NO}_3)_2$ ,  $\text{NH}_4\text{H}_2\text{PO}_4$ , and citric acid ( $\text{C}_6\text{H}_8\text{O}_7$ ) in a 1:1:1:1 molar ratio were dissolved in distilled water. After complete dissolution of starting materials, the obtained solution was heated with continuous stirring at  $80^\circ\text{C}$  for 2 h then the hot plate temperature was set at  $120^\circ\text{C}$ . After 12 h reaction, a gel-like specimens resin was

obtained. For pretreatment of samples, the gel-like matter was subjected to pyrolysis at 350 °C for 2 h in air atmosphere. The resulting carbonate precursor was calcinated at 500 °C for 5 h in air and the LiCoPO<sub>4</sub> particles were obtained. Then, the obtained powder was ground with LiF in ethanol in a agate mortar for 30 minutes for evaporation of ethanol. The dry mixed powder is pelletized and calcined at 700 °C for 2 h in Ar atmosphere, followed by the natural cooling to room temperature.

The crystalline phase of the samples were characterized using powder X-ray diffraction (XRD; Rigaku RINV-2200, 40 kV and 30 mA) with CuK $\alpha$  radiation ( $\lambda = 1.5406 \text{ \AA}$ ). Data were collected in the 2 $\theta$ - $\theta$  scanning mode with a scan speed of 4° min<sup>-1</sup> and a step size of 0.02°. HRTEM and HAADF images, elemental mapping, EDS spectra were collected using JEOL JEM-2100F. The synthesized particles were dry in vacuum before the characterization to prevent any chemical reaction which might occurs in air. Samples for TEM observation were dispersed in ethanol by sonication for a minute and then dropped onto Cu microgrid coated with a holey carbon film, followed by evaporation of ethanol in vacuum. Camera length is 6 cm; BF aperture is 3 cm and HAADF detector spanned the range of 70 to 180 mrad. Fourier transform infrared spectroscopy (FTIR) spectra were recorded with a FT/IR 6200 spectrophotometer (JASSO, Japan) within the range of 400–4000 cm<sup>-1</sup>. Samples in the solid state were measured in KBr matrix pellets were obtained with hydraulic press under 40 kN pressure. Raman spectra were evaluated in the range of 400–2000 cm<sup>-1</sup> using NRS-3100, JASSO, Japan.

The electrochemical performance of Li<sub>2</sub>CoPO<sub>4</sub>F was investigated using coin-type cells (CR2032). The working electrodes is composed of 80 wt.% Li<sub>2</sub>CoPO<sub>4</sub>F, 10 wt.%

PTFE (poly(tetrafluoroethylene)) as a binder and 10 wt.% acetylene black. These materials were ground by conventional agate mortar to make electrode paste. The prepared paste was spread uniformly, rolling into sheet then dried in a vacuum oven for 4 h at 160 °C. The cathode sheet was punched into circular discs and cut into wafers (7 mm in diameter, 0.025mm in thickness, 5-6 mg). The tested cell was assembled inside an argon-filled glove box. For electrochemical measurements, the cell is composed of lithium metal counter, reference electrodes and a  $\text{Li}_2\text{CoPO}_4\text{F}$  positive electrode. The cathode and reference electrodes were separated by a microporous polypropylene film. 1 M solution of  $\text{LiPF}_6$  in a mixed solvent of ethylene carbonate (EC), diethylene carbonate (DEC) and dimethyl carbonate (DMC) with 1:1:3 in volume ratio (Tomiyama Pure Chemical Co., Ltd.) was used as the electrolyte. The charge-discharge cycling were performed galvanostatically between 3.0 and 5.1 V or 5.5 V versus  $\text{Li}/\text{Li}^+$  on multi-channel battery testers (Hokuto Denko, Japan) at various charge/discharge rates ranging from 0.1 to 1 C (1 C = 144  $\text{mA}\text{h}^{-1}$ , assuming that only one Li can be retracted and inserted). Current densities and specific capacities were calculated on the basis of the weight of  $\text{Li}_2\text{CoPO}_4\text{F}$  cathode in the electrode.

### 3. Results and discussion

#### 3.1. Material characterization

The  $\text{Li}_2\text{CoPO}_4\text{F}$  structure is composed of chain of edge-sharing  $\text{CoO}_4\text{F}_2$  octahedral, and each octahedral is interconnected with a  $\text{PO}_4$  tetrahedral oxo-anion by corner sharing (Fig. 1). The cross-linked structure forms opened three-dimensional frameworks, allowing Li ions are inserted and extracted along multi directions which differs from

that of olivine structure with one dimensional diffusion path [21].

The TEM image in Fig. 2a shows that the synthesized  $\text{Li}_2\text{CoPO}_4\text{F}$  are of micron sized particles. Fig. 2b, c, d show the selected-area electron diffraction pattern and the HR-TEM images of a typical particle, respectively. SAED pattern taken from the particle can be indexed to the [010] zone axis of single-crystal  $\text{Li}_2\text{CoPO}_4\text{F}$  structure. The diffraction maxima are due to the reflections from the lattice planes of {200} and {002} of the  $\text{Li}_2\text{CoPO}_4\text{F}$  structure in orthorhombic crystal system (Fig. 2b). It was found that  $\text{Li}_2\text{CoPO}_4\text{F}$  was very sensitive to electron beam of HRTEM mode as it was decomposed during the observation. Thus, the observation was acquired for a short time. The HR-TEM images in Fig. 2c, d are formed by parallelograms of the brightest dots arranged into layers along the *c* axis and into staggered configuration along the *a* axis similar to observation by Hadermann et al.<sup>16</sup> The lattice fringes spacing calculated from TEM image and SAED are 0.53 nm along [100] direction and 0.55 nm along [001] direction which are in good agreement with the calculation from XRD data and precession electron diffraction [16,18]. The observed lattice fringe spacing are attributed to the (200) and (002) plane spacing, indicating that the particle is viewed from [010] direction. That is consistent with the corresponding electron diffraction pattern in Fig. 2b. Fig. 3 shows TEM images and SAED patterns of the different particles, indexed to [100] zone axis of the  $\text{Li}_2\text{CoPO}_4\text{F}$  structure. The ED patterns can be assigned with orthorhombic unit cell.

Fig. 4 shows HAADF-STEM image of bulk and surface of a  $\text{Li}_2\text{CoPO}_4\text{F}$  particle. Because the ADF image contrast is roughly correlates with atomic number according to a  $Z^{1.7}$  relationship [21], Co (Z=27), the most heavy atom in the structure, can be

visualized even at low resolution of HAADF mode. Thus, the bright contrast in Fig. 4 demonstrates the chain of Co atomic columns. The direct space TEM observation exhibits the chain of Co atom in a continuous bright line. The distance between these bright lines is 0.52 nm, indicating that the particle is viewed from [010] direction. The attempt to observe the structure at higher magnification was unsuccessful due to the fact that  $\text{Li}_2\text{CoPO}_4\text{F}$  is very sensitive to electron beam. Thus, STEM image with atomic resolution was not observed in this study.

Furthermore, to verify that the chemical composition of the synthesized particles, the EDS analysis and elemental mapping of the  $\text{Li}_2\text{CoPO}_4\text{F}$  sample by STEM were conducted. EDS elemental mappings by STEM (Fig. 5b-d) showed a uniform distribution of Co, P, O, F and the EDS spectrum of the sample exhibits the characteristic peaks of Co, P, O, F, indicating the  $\text{Li}_2\text{CoPO}_4\text{F}$  phase purity in the synthesized particles. No other element was detected in EDS analysis by STEM. The micro-scale analysis of the sample by SEM-EDS further supports above conclusion and provide the elemental composition of the synthesized  $\text{Li}_2\text{CoPO}_4\text{F}$  powder (Table S1, Fig. S1). These characterizations confirm the purity, homogeneity and uniform elemental distribution in the obtained particles. More importantly, the presence of F was confirmed, indicating the successful formation of  $\text{Li}_2\text{CoPO}_4\text{F}$ .

The XRD pattern of the synthesized  $\text{Li}_2\text{CoPO}_4\text{F}$  particles is shown in Fig. 6. All diffraction peaks were indexed to orthorhombic unit cell with *Pnma* space group and  $a = 10.4520 \text{ \AA}$ ,  $b = 6.3911 \text{ \AA}$ ,  $c = 10.8740 \text{ \AA}$ , in agreement with reported values [13,16,18]. It is evident from the XRD pattern that single phase of  $\text{Li}_2\text{CoPO}_4\text{F}$  has been prepared.

Raman spectrum of the synthesized  $\text{Li}_2\text{CoPO}_4\text{F}$  particles shows a strong signal at  $973 \text{ cm}^{-1}$  which can be assigned to intramolecular symmetric vibrations of the P–O in phosphate oxo-anion (singlet  $A_1$  at frequency  $\nu_1 = 973 \text{ cm}^{-1}$ ) (Fig. 7a). The other band at  $1057 \text{ cm}^{-1}$  is due to the asymmetric stretching modes of the P–O bonds (triplet  $F_2$  mode,  $\nu_3$ ). The bands observed between  $400$  and  $700 \text{ cm}^{-1}$  are ascribed to the symmetric and asymmetric bending modes of O–P–O (doublet E mode,  $\nu_2$  and triplet  $\nu_4$ ). The Raman spectrum of the  $\text{LiCoPO}_4$  is also records for comparison as shown in Fig. 7a. Notably, the symmetric stretching vibration band in  $\text{PO}_4^{3-}$  of  $\text{Li}_2\text{CoPO}_4\text{F}$  are blue-shift. The origin of blue-shift is unknown and needs further investigation. FTIR spectra of the synthesized  $\text{Li}_2\text{CoPO}_4\text{F}$  particles were also investigated to clarify the local structure and chemical bonding. Fig. 7b shows the FTIR spectra of  $\text{Li}_2\text{CoPO}_4\text{F}$  in comparison with that of  $\text{LiCoPO}_4$  (Table 1). Similarly, the FTIR peaks of  $\text{PO}_4^{3-}$  can be found such as an symmetric stretching vibration mode at  $983 \text{ cm}^{-1}$  ( $\nu_1$ ), a doublet at around  $471 \text{ cm}^{-1}$  ( $\nu_2$ ) and two triplets ( $\nu_3$  and  $\nu_4$ ) in the region  $1029– $1130 \text{ cm}^{-1}$  and at  $625 \text{ cm}^{-1}$ . Comparing to that of  $\text{LiCoPO}_4$ , the symmetric stretching vibration mode  $\nu_1$  is almost disappeared, revealing the rise of symmetry of  $\text{PO}_4$  tetrahedral in the  $\text{Li}_2\text{CoPO}_4\text{F}$  structure due to the introduction of F ions [17].$

### 3.2. Electrochemical performance

The electrochemical performance of the synthesized  $\text{Li}_2\text{CoPO}_4\text{F}$  has been measured by galvanostatic charge-discharge in  $\text{LiPF}_6/\text{EC+DEC+DMC}$  electrolyte and the result is shown in Fig. 8. The first measurement was performed between  $3 \text{ V}$  and  $5.1 \text{ V}$  versus  $\text{Li}/\text{Li}^+$  (Fig. 8a). The  $\text{Li}_2\text{CoPO}_4\text{F}$  exhibited a slope voltage plateau at around  $4.8 \text{ V}$

versus Li/Li<sup>+</sup> with a initial discharge capacity of 52 mAhg<sup>-1</sup> at C/10 rate. In order to deintercalate more amount of Li ions, the electrochemical test was carried out between 3 V and 5.5 V versus Li/Li<sup>+</sup>. The cyclic voltammogram curve up to 5.5 V of the sample is shown in Fig. 8b. The curve exhibits two oxidative peaks at 4.85 V and 5.18 V and one broaden reductive peak centered at 4.73 V. The discharge curve shows a discharge voltage at around 5.0 V versus Li/Li<sup>+</sup> with initial discharge capacity of 91 mAhg<sup>-1</sup> which is comparable to the result in the previous reports [14,16,19]. It should be noted that the charge capacity exceeds the theoretical capacity owing to the decomposition of the electrolyte at high voltage (Fig. S2) [19]. The slope plateau indicates that deintercalation mechanism differs from that of LiCoPO<sub>4</sub> [14–16,19,20]. Fig. 8c exhibits the cyclic performance of the cell. The discharge capacity of Li<sub>2</sub>CoPO<sub>4</sub>F is 68 mAhg<sup>-1</sup> at 20 cycle with a current rate of 0.1 C and the capacity retention is about 75%. The Li<sub>2</sub>CoPO<sub>4</sub>F cathodes showed much better cyclic performance compared to that of LiCoPO<sub>4</sub> [21]. That may due to the intrinsic structural features of the former with opened frameworks and multi diffusion pathway. Fig. 8d presents the rate capacity of the cells containing Li<sub>2</sub>CoPO<sub>4</sub>F at various discharge rates ranging from 0.1 C to 2 C. The cell exhibited initial discharge capacity of 91, 75, 69, 53 mAhg<sup>-1</sup> at 0.1, 0.5, 1, 2 C, respectively. At high discharge rate of 2 C, the cell exhibited a reduced discharge voltage at 4.5 V and decreased discharge capacity of 53 mAhg<sup>-1</sup>. This may be due to the fact that the selective electrochemical reaction on the particle surface occurs at high current rate [19].

#### 4. Conclusions

$\text{Li}_2\text{CoPO}_4\text{F}$  has been successfully prepared by a modified sol-gel method combining with solid state reaction. The XRD pattern of  $\text{Li}_2\text{CoPO}_4\text{F}$  particles could be identified as single phase, indexed by orthorhombic *Pnma* crystal system. The calculated lattice parameters were well-agreed with the calculated data from other methods reported in literature. The well-resolved uniform lattice fringes observed from HRTEM image reveal that the synthesized  $\text{Li}_2\text{CoPO}_4\text{F}$  particles are highly crystalline and free of defects. The SAED pattern recorded with different electron beam directions indicate that the compound crystallized in orthorhombic crystal system. The  $\text{Li}_2\text{CoPO}_4\text{F}$  structure was also visualized using HAADF-STEM with observation of Co atomic chains. The elemental mapping by HAADF-STEM confirms the purity, homogeneity and uniform elemental distribution in the obtained particles. The  $\text{Li}_2\text{CoPO}_4\text{F}$  particles were used as cathode materials for lithium batteries, and the cells exhibited initial discharge capacities of 91, 75, 69, 53  $\text{mA}\text{h}^{-1}$  at 0.1, 0.5, 0.1, 2 C, respectively. Due to its stability at high voltage, the  $\text{Li}_2\text{CoPO}_4\text{F}$  material may have good potential for practical application as a high-energy density cathode materials.

### **Acknowledgements**

This research work was financially supported by NEDO, Japan. Q. D. Truong would like to acknowledge the Japan Society for Promotion of Science (JSPS), Japan for awarding fellowship, Grant No. 13070.

### **References**

- [1] M. K. Devaraju, I. Honma, Hydrothermal and solvothermal process towards development of  $\text{LiMPO}_4$  ( $\text{M} = \text{Fe, Mn}$ ) nanomaterials for lithium-ion batteries. *Adv. Energy Mater.* 2 (2012) 284.

[2] R. Dinesh, M. K. Devaraju, T. Tomai, A. Unemoto, I. Honma, Ultrathin nanosheets of  $\text{Li}_2\text{MSiO}_4$  (M = Fe, Mn) as high-capacity Li-ion battery electrode. *Nano Lett.* 12 (2012) 1146.

[3] P. Barpanda, M. Ati, B.C. Melot, G. Rousse, J-N. Chotard, M-L. Doublet, M.T. Sougrati, S.A. Corr, J-C. Jumas, J-M. Tarascon, A 3.90 V iron-based fluorosulphate material for lithium-ion batteries crystallizing in the triplite structure. *Nature Mater.* 10 (2011) 772.

[4] R. Tripathi, G. Popov, B.L. Ellis, A. Huq, L.F. Nazar, Lithium metal fluorosulfate polymorphs as positive electrodes for Li-ion batteries: synthetic strategies and effect of cation ordering. *Energy Environ. Sci.* 5 (2012) 6238.

[5] Y. U. Park, D. H. Seo, B. Kim, K. P. Hong, H. Kim, S. Lee, R. A. Shakoor, K. Miyasaka, J. M. Tarascon, K. Kang, Tailoring a fluorophosphate as a novel 4 V cathode for lithium-ion batteries. *Sci. Rep.* 2 (2012) 704.

[6] J. Barker, M.Y. Saidi, R.K.B. Gover, P. Burns, A. Bryan, The effect of Al substitution on the lithium insertion properties of lithium vanadium fluorophosphate,  $\text{LiVPO}_4\text{F}$ . *J. Power Sources* 174 (2007) 927.

[7] Y. Makimura, L.S. Cahill, Y. Iriyama, G.R. Goward, L.F. Nazar, Layered Lithium Vanadium Fluorophosphate,  $\text{Li}_5\text{V}(\text{PO}_4)_2\text{F}_2$ : A 4V Class Positive Electrode Material for Lithium-Ion Batteries. *Chem. Mater.* 20 (2008) 4240.

[8] T.N. Ramesh, K.T. Lee, B.L. Ellis, L.F. Nazar, Tavorite Lithium Iron Fluorophosphate Cathode Materials: Phase Transition and Electrochemistry of  $\text{LiFePO}_4\text{F}$ - $\text{Li}_2\text{FePO}_4\text{F}$ . *Electrochem. Solid-State Lett.* 13 (2010) A43.

[9] N. Recham, J.N. Chotard, J.C. Jumas, L. Laffont, M. Armand, J.M. Tarasco, Ionothermal Synthesis of Li-Based Fluorophosphates Electrodes. *Chem. Mater.* 22 (2010) 1142.

[10] B.L. Ellis, W.R.M. Makahnouk, W.N. Rowan-Weetaluktuk, D.H. Ryan, L.F. Nazar, Crystal Structure and Electrochemical Properties of  $A_2MPO_4F$  Fluorophosphates ( $A = Na, Li$ ;  $M = Fe, Mn, Co, Ni$ ). *Chem. Mater.* 22 (2010) 1059.

[11] S.-W. Kim, D.-H. Seo, H. Kim, K.-Y. Park, K. Kang, A comparative study on  $Na_2MnPO_4F$  and  $Li_2MnPO_4F$  for rechargeable battery cathodes. *Phys. Chem. Chem. Phys.* 14 (2012) 3299.

[12] M. Nagahama, N. Hasegawa, S. Okada, High Voltage Performances of  $Li_2NiPO_4F$  Cathode with Dinitrile-Based Electrolytes. *J. Electrochem. Soc.* 157 (2010) A748.

[13] S. Okada, M. Ueno, Y. Uebou, J. Yamaki, Fluoride phosphate  $Li_2CoPO_4F$  as a high-voltage cathode in Li-ion batteries. *J. Power Sources* 146 (2005) 565.

[14] E. Dumont-Botto, C. Bourbon, S. Patoux, P. Rozier and M. Dolle, Synthesis by Spark Plasma Sintering: A new way to obtain electrode materials for lithium ion batteries. *J. Power Sources* 196 (2011) 2274.

[15] N.R. Khasanova, A.N. Gavrilov, E.V. Antipov, K.G. Bramnik, H. Hibst, Structural transformation of  $Li_2CoPO_4F$  upon Li-deintercalation. *J. Power Sources* 196 (2011) 355.

[16] D. Wang, J. Xiao, W. Xu, Z. Nie, C. Wang, G. Graff, J.G. Zhang, Preparation and electrochemical investigation of  $Li_2CoPO_4F$  cathode material for lithium-ion batteries. *J. Power Sources* 196 (2011) 2241.

[17] N.V. Kosova, E.T. Devyatkina, A.B. Slobodyuk, In situ and ex situ X-ray study of formation and decomposition of  $Li_2CoPO_4F$  under heating and cooling. Investigation of its local structure and electrochemical properties. *Solid State Ion.*, 225 (2012) 570.

[18] J. Hadermann, A.M. Abakumov, S. Turner, Z. Hafideddine, N.R. Khasanova, E.V. Antipov, G.V. Tendeloo, Solving the structure of Li ion battery materials with

precession electron diffraction: Application to  $\text{Li}_2\text{CoPO}_4\text{F}$ . *Chem. Mater.* 23 (2011) 3540.

[19] S. Amaresh, G.J. Kim, K. Karthikeyan, V. Aravindan, K.Y. Chung, B.W. Cho, Y.S. Lee, Synthesis and enhanced electrochemical performance of  $\text{Li}_2\text{CoPO}_4\text{F}$  cathodes under high current cycling. *Phys. Chem. Chem. Phys.* 14 (2012) 11904.

[20] X. Wu, Z. Gong, S. Tan, Y. Yang, Sol-gel synthesis of  $\text{Li}_2\text{CoPO}_4\text{F}/\text{C}$  nanocomposite as a high power cathode material for lithium ion batteries. *J. Power Sources* 220 (2012) 122.

[21] Q. D. Truong, M. K. Devaraju, T. Tomai, I. Honma, Direct observation of antisite defects in  $\text{LiCoPO}_4$  cathode materials by annular dark- and bright-field electron microscopy. *ACS Appl. Mater. Interfaces* 5 (2013) 9926.

**Table 1.** Infrared vibrational assignments

Vibrational modes	Mode	Frequency ( $\text{cm}^{-1}$ )	
		$\text{Li}_2\text{CoPO}_4\text{F}$	$\text{LiCoPO}_4$
$\nu_{\text{as}}(\text{PO}_4)$	triplet $\nu_3$	1030	1028
$\nu_{\text{s}}(\text{PO}_4)$	singlet $\nu_1$	983	962
$\delta_{\text{as}}(\text{PO}_4)$	triplet $\nu_4$	625, 590	642, 589
$\delta_{\text{s}}(\text{PO}_4)$	doublet $\nu_2$	471	472

$\nu_{\text{as}}$  = asymmetric stretching vibration;  $\nu_{\text{s}}$  = symmetric stretching vibration;  $\delta$  = bending vibration.

## Figure captions

**Fig. 1.** (a, b) Crystal structure of  $\text{Li}_2\text{CoPO}_4\text{F}$  view along [010] and [011] different directions, respectively. (c) Illustration of  $\text{CoO}_4\text{F}_2$  octahedral and  $\text{PO}_4$  tetrahedral.

**Fig. 2.** (a) TEM image, (b) SAED pattern, (c, d) HRTEM images of the synthesized  $\text{Li}_2\text{CoPO}_4\text{F}$  particle.

**Fig. 3.** (a, c) TEM images of the  $\text{Li}_2\text{CoPO}_4\text{F}$  particle and (b, d) the corresponding SAED patterns of the particles.

**Fig. 4.** HAADF-STEM image of  $\text{Li}_2\text{CoPO}_4\text{F}$  particle.

**Fig. 5.** (a) STEM image, (b, c, d, e) Elemental mapping of O, F, P, Co respectively and (e) EDS spectrum of the synthesized  $\text{Li}_2\text{CoPO}_4\text{F}$  particles by STEM analysis.

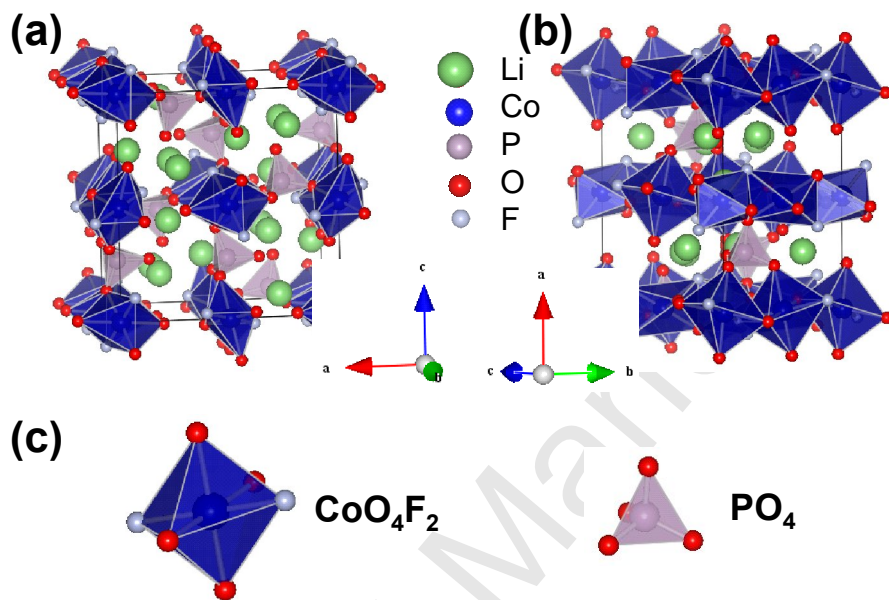
**Fig. 6.** (a) XRD pattern of the synthesized  $\text{Li}_2\text{CoPO}_4\text{F}$ .

**Fig. 7.** (a) Raman spectra and (b) FTIR spectra pattern of (i) the synthesized  $\text{Li}_2\text{CoPO}_4\text{F}$ , (ii) the synthesized  $\text{LiCoPO}_4$ .

**Fig. 8.** Electrochemical performances of the synthesized  $\text{Li}_2\text{CoPO}_4\text{F}$  in Li-ion batteries: (a) typical first charge/discharge profiles tested in the potential range of 3.0–5.1 V (i) and 3.0–5.5 V (ii); (b) cyclic voltammograms of the cells in the potential range of 3.0–5.1 V (i) and 3.0–5.5 V (ii); (c) cyclic performance of  $\text{Li}_2\text{CoPO}_4\text{F}$  at 0.1 C rate and

(c) the initial discharge curves of  $\text{Li}_2\text{CoPO}_4\text{F}$  at different current rates.

Accepted Manuscript

**Figure and Captions**

**Fig. 1.** (a, b) Crystal structure of  $\text{Li}_2\text{CoPO}_4\text{F}$  view along [010] and [011] different directions, respectively. (c) Illustration of  $\text{CoO}_4\text{F}_2$  octahedral and  $\text{PO}_4$  tetrahedral.

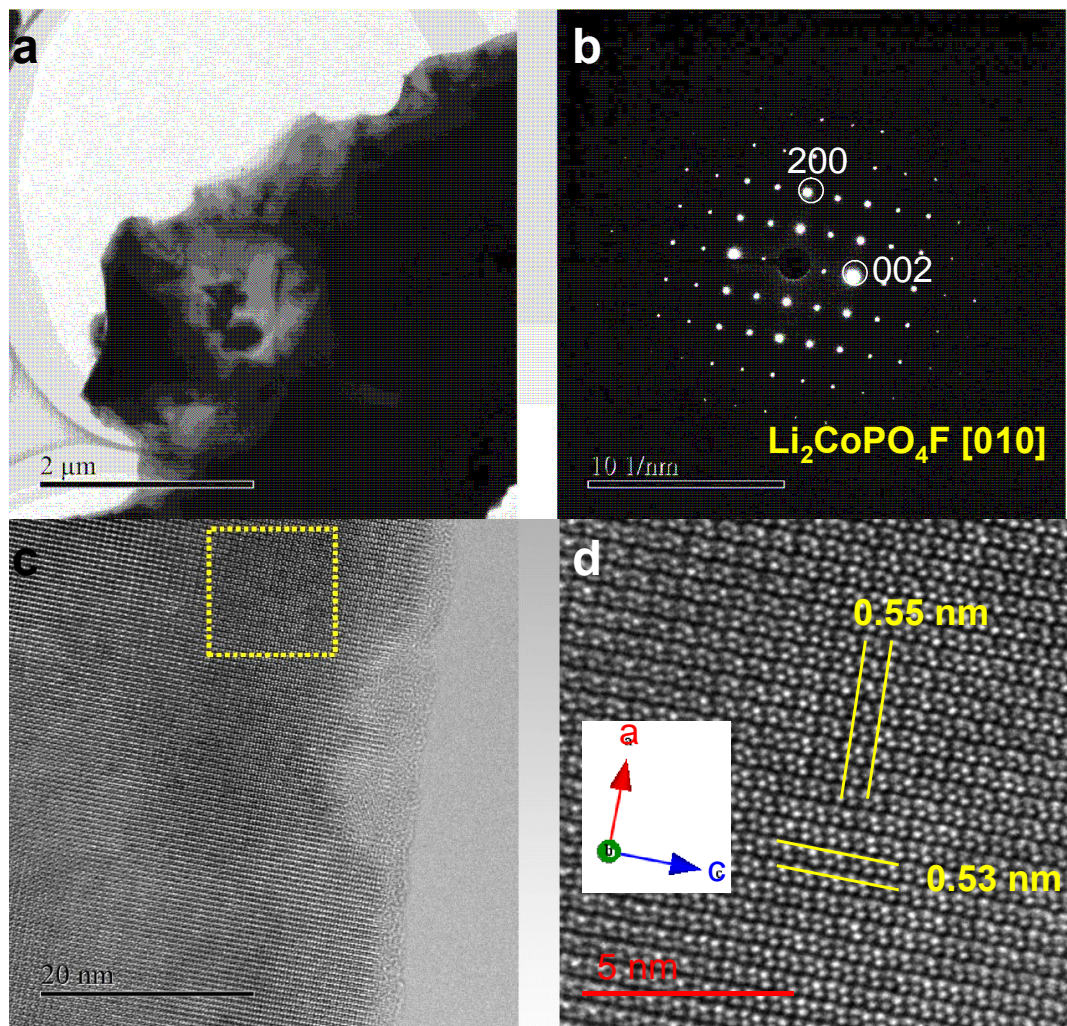


**Fig. 2.** (a) TEM image, (b) SAED pattern, (c, d) HRTEM images of the synthesized Li<sub>2</sub>CoPO<sub>4</sub>F particle.

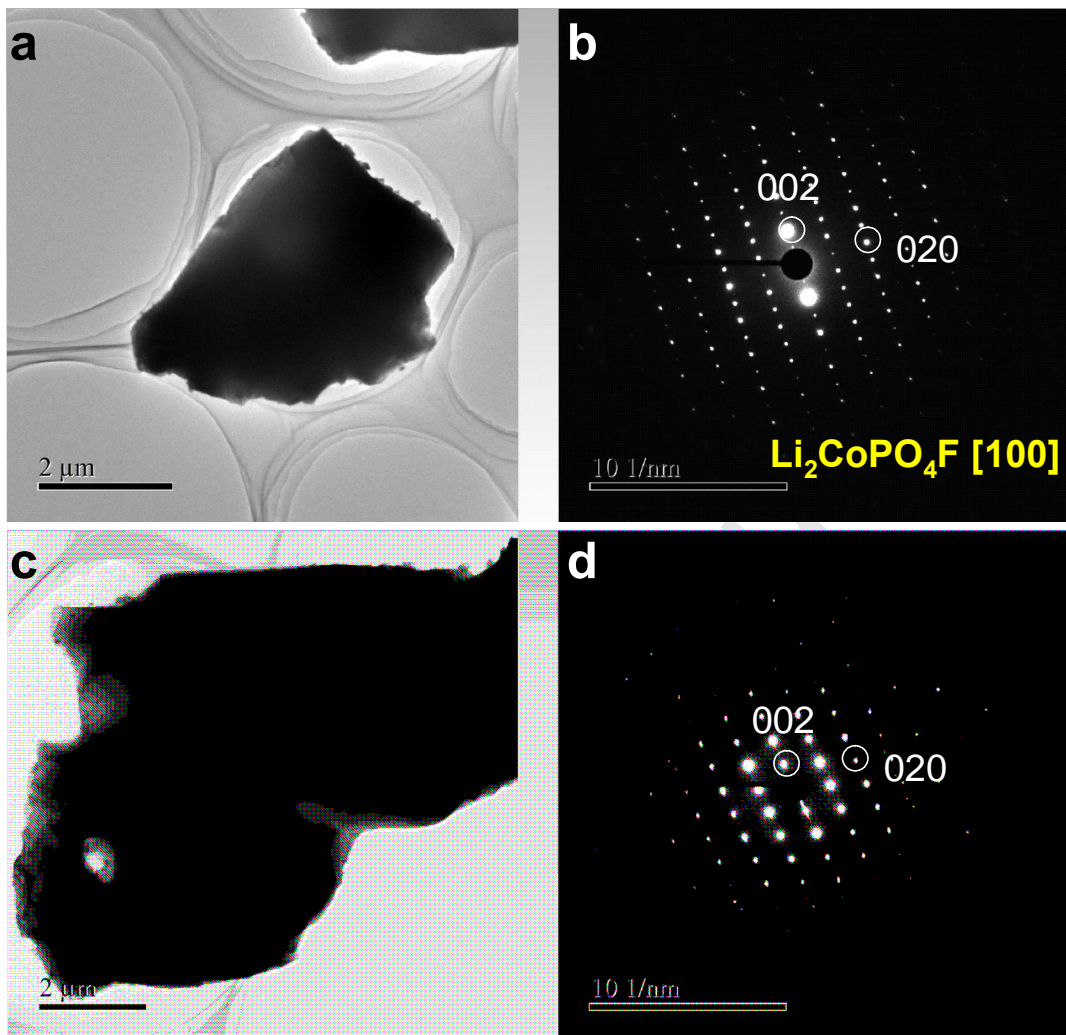


**Fig. 3.** (a, c) TEM images of the  $\text{Li}_2\text{CoPO}_4\text{F}$  particles and (b, d) the corresponding SAED patterns of the particles.

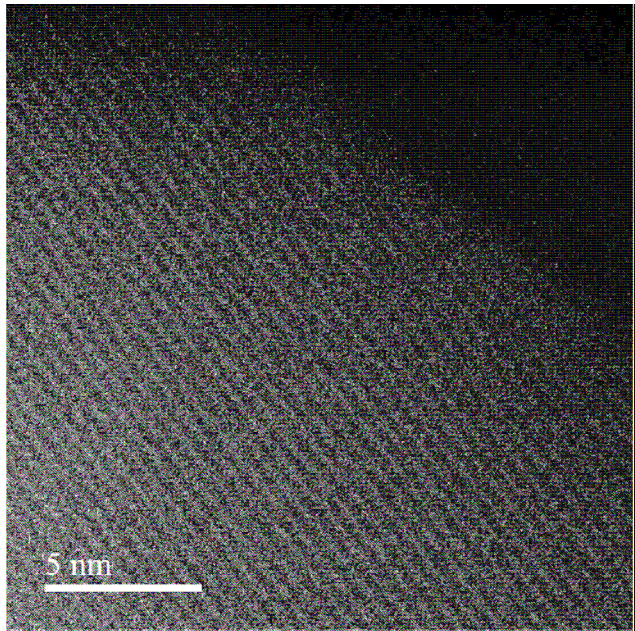


**Fig. 4.** HAADF-STEM image of  $\text{Li}_2\text{CoPO}_4\text{F}$  particle.

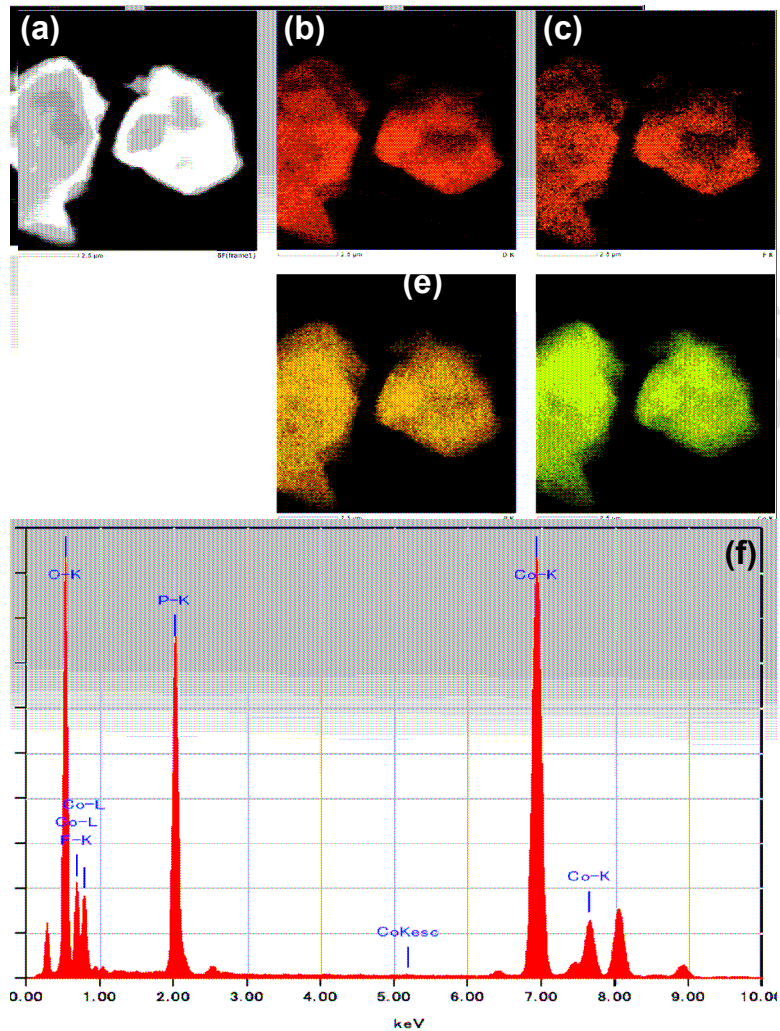


**Fig. 5.** (a) STEM image, (b, c, d, e) Elemental mapping of O, F, P, Co respectively and (e) EDS spectrum of the synthesized  $\text{Li}_2\text{CoPO}_4\text{F}$  particles by STEM analysis.

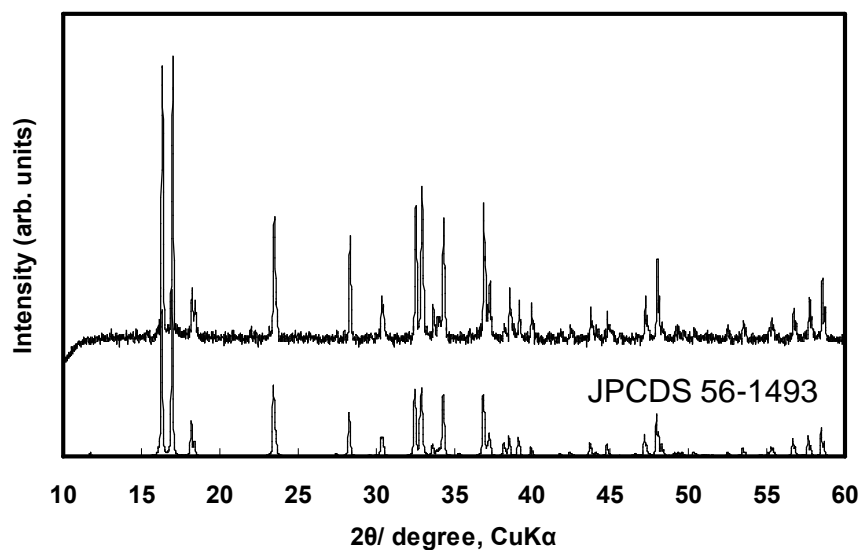


**Fig. 6.** (a) XRD pattern of the synthesized  $\text{Li}_2\text{CoPO}_4\text{F}$ .

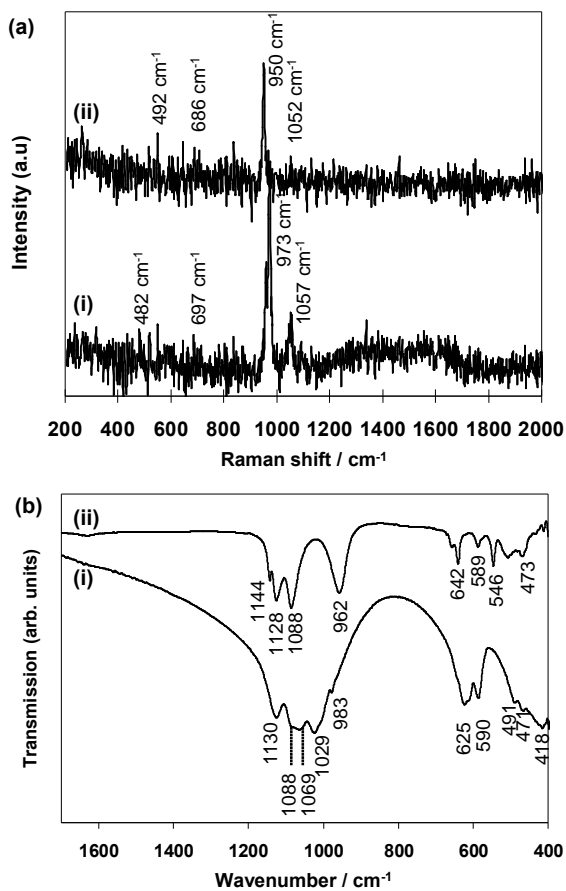


**Fig. 7.** (a) Raman spectra, (b) FTIR spectra pattern of (i) the synthesized  $\text{Li}_2\text{CoPO}_4\text{F}$  and (ii) the synthesized  $\text{LiCoPO}_4$ .

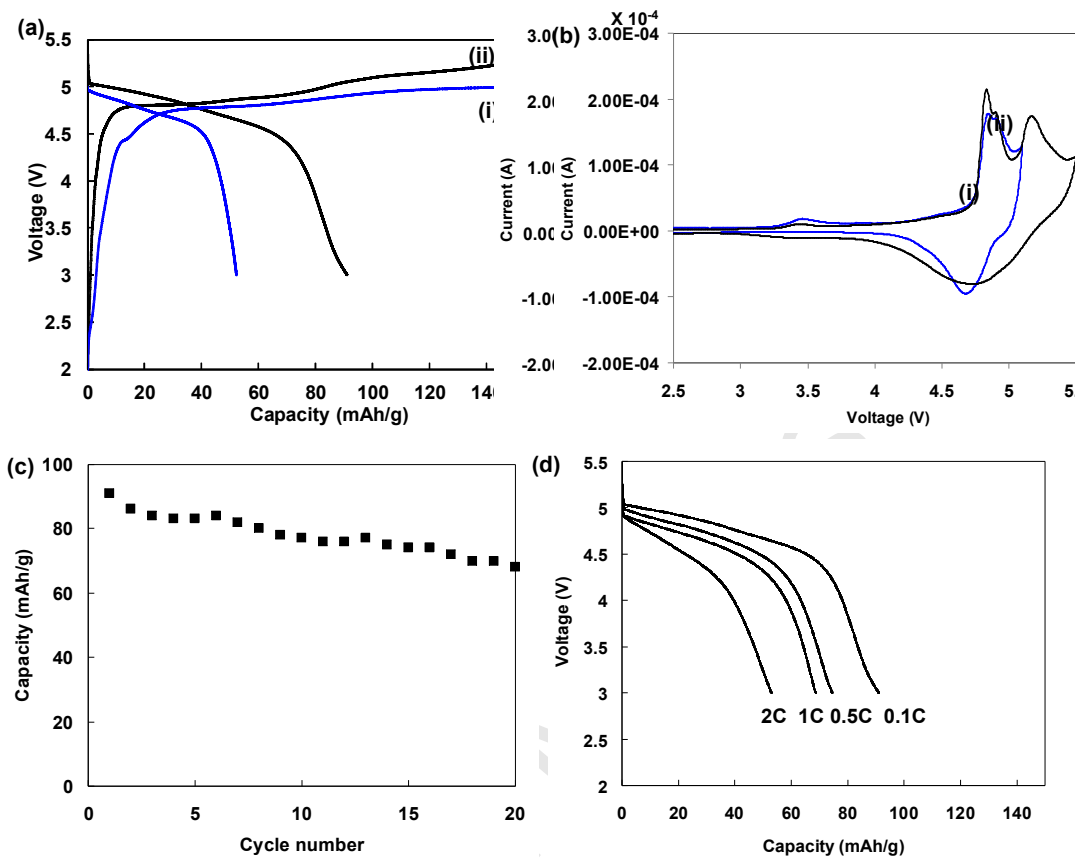


**Fig. 8.** Electrochemical performances of the synthesized  $\text{Li}_2\text{CoPO}_4\text{F}$  in Li-ion batteries:  
 (a) typical first charge/discharge profiles tested in the potential range of 3.0–5.1 V (i) and 3.0–5.5 V (ii); (b) cyclic voltammograms of the cells in the potential range of 3.0–5.1 V (i) and 3.0–5.5 V (ii); (c) cyclic performance of  $\text{Li}_2\text{CoPO}_4\text{F}$  at 0.1 C rate and (c) the initial discharge curves of  $\text{Li}_2\text{CoPO}_4\text{F}$  at different current rates.